

WEIDLINGER ASSOCIATES, CONSULTING ENGINEERS

110 EAST 59TH STREET
NEW YORK, NEW YORK 10022

and

SUITE 245, BUILDING 4
3000 SAND HILL ROAD
MENLO PARK, CALIFORNIA 94025

DYNAMIC RESPONSE OF AN EMBEDDED PIPE
SUBJECTED TO PERIODICALLY SPACED LONGITUDINAL FORCES

by

R. Parnes and P. Weidlinger

Grant Report No. 13

Prepared for
National Science Foundation (ASRA Directorate)
1800 G Street
Washington, D.C. 20550

Grant No. PFR 78-15049

August 1979

*Any opinions, findings, conclusions
or recommendations expressed in this
publication are those of the author(s)
and do not necessarily reflect the views
of the National Science Foundation.*



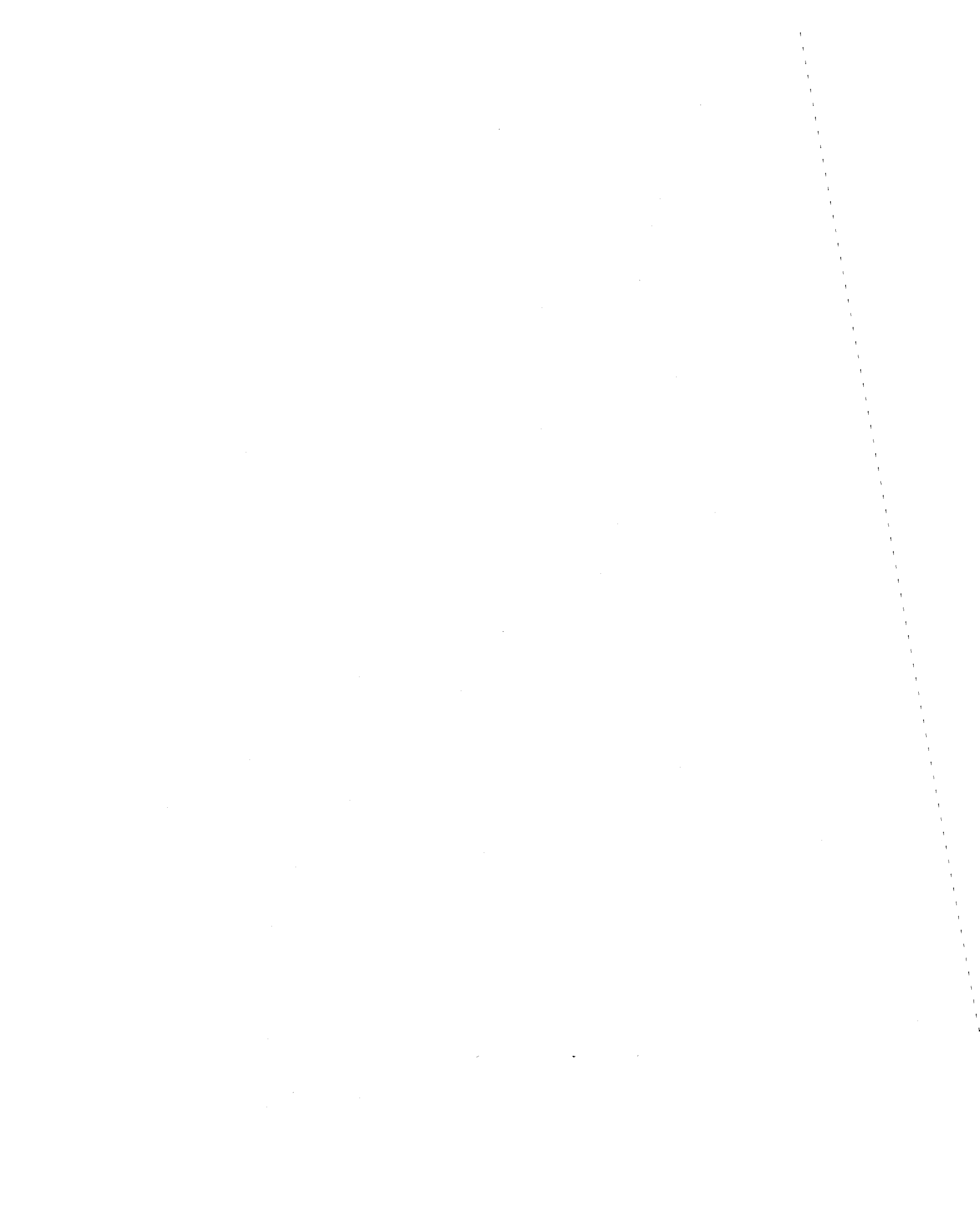
ABSTRACT

The dynamic response of pipe systems buried in soil is studied. The degree of interaction between the pipe and surrounding soil as well as the amount of damping is established for pipes subjected to incoherent motion. The model considered is represented by a pipe of diameter D subjected to time-harmonic longitudinal forces acting periodically at intervals L in alternating directions. Such a loading pattern corresponds to the incoherent component of earthquake excitation.

The pipe and the soil are assumed to behave as linear isotropic elastic materials and the interaction between the surrounding soil and pipe is assumed to occur through a shear force mechanism acting at the pipe-soil interface. The response is found to be expressible in terms of non-dimensional ratios of density, velocity of wave propagation and the aspect ratio D/L of the pipe.

Results are presented in terms of dynamic amplification factors for various applied frequencies of the applied forces. Peak response and resonant frequencies are determined and regions where radiation damping occurs are established.

By choosing the suitable values of the governing parameters judiciously, the response can be obtained for either a continuous pipe or for an infinite train of pipe segments, interconnected by elastic joints at intervals L .



I. INTRODUCTION

The effect of earthquakes on lifeline systems has received considerable attention in recent years [1-3]. One question of concern is the dynamic response of pipe systems buried in soil and subjected to earthquakes. Among the most important facts to be established are the degree of interaction between the pipe and surrounding soil and the amount of damping, if any, which takes place in the system. Inertial effects are generally considered to be negligible [4-5], leading to the conclusion that the pipes follow the free-field motion. In the present report, it is shown that the dynamic interactive effect can be considerable, resulting in large dynamic amplification particularly for pipes whose diameters are not small compared to the predominant wave lengths in earthquakes.

The axial displacement response of buried pipes to earthquake excitation can be conveniently studied by response spectral techniques [6], provided that the dynamic response parameters of the pipe-soil medium system are available.

In this study, the response of an infinite train of pipe segments of diameter D , interconnected by elastic joints at intervals L , is considered, (Fig. 1). The periodic, longitudinal axial forces act at the joints at intervals L . Since the relevant seismic input on the pipe is the incoherent component of the excitation [6], these forces are taken in alternating directions. The model, therefore, is assumed

to be an infinite pipe subjected to periodically spaced forces as shown in Fig. (2). The pipe as well as the soil are assumed to behave as linear isotropic elastic materials and the interaction between the surrounding soil and pipe is assumed to occur through a shear force mechanism acting at the soil-pipe interface which prevents slip at the pipe-soil interface.

To simulate the realistic condition of a jointed pipe, the effect of the joints (which are much more flexible than the pipe material itself) is taken into account in determining the average overall longitudinal stiffness of the pipe. Since the radial displacements of the pipe are known to be small, for mathematical simplicity, the pipe is assumed to be radially rigid. Such an assumption has been used previously [7].

Numerical results of the analysis are presented for a pipe buried in a typical soil where c_s , the propagation velocity of S-waves, is 400 ft/sec and for which Poisson's ratio $\nu = 0.3$. It is seen that the response can be expressed in terms of several non-dimensional ratios of density and velocity of wave propagation. The response is also seen to depend strongly on the aspect ratio D/L of the pipe. Responses to several such pipes are obtained as a function of the forcing frequency of the applied force.

In order to demonstrate the dynamic effect of the earthquake, results are presented in terms of a dynamic amplification factor (DAF) defined as the ratio of dynamic to corresponding static response.

A subject of major interest is the determination of peak responses which occur at resonant frequencies. Resonance occurs when the forcing frequency coincides with the frequency of an excited wave of specific wave

length in the system. (It is noted that corresponding to any given wave length, propagation can occur only at certain discrete frequencies. Such frequency-wave length relations are a result of the dispersive character of the system.) Frequency ranges are established where no radiation damping occurs and it is observed that in this range, the response contains infinite DAF.

From the study of the analytic solution and observation of the numerical results obtained, several general conclusions are established which govern the response of the pipe-soil system.

II. GENERAL FORMULATION AND SOLUTION

The model considered represents an infinite cylindrical pipe of radius a , embedded in soil and which is subjected to dynamic concentrated forces $F(t)$, acting in the longitudinal z -direction at periodic intervals L as shown in Fig. (2). The forces are assumed to act harmonically in time with frequency f .

The pipe is represented by means of an equivalent solid cylindrical bar of cross-sectional area A with modulus of elasticity \bar{E} , and density $\bar{\rho}$, whose motion in the longitudinal z -direction is denoted by $U_p(z,t)$. Following the assumption of radial rigidity [7], the radial displacements are taken as zero throughout the pipe.

The surrounding medium is assumed to behave as a linear elastic material having density ρ and defined by a shear modulus μ and Poisson ratio ν . For the axi-symmetric case considered here, the soil medium can undergo time-dependent radial and axial displacements denoted by $U_r(r,z,t)$ and $U_z(r,z,t)$ respectively.

The interaction between the pipe and surrounding medium is then due to an interactive shear force mechanism, acting along the pipe-soil cylindrical interface, which prevents slip between pipe and soil.

Denoting the harmonically applied periodic concentrated forces by means of periodically spaced Dirac-delta functions $\delta_p(z)$, the force $F(t)$ is represented by

$$F(t) = F_0 \delta_p(z) e^{-i\omega t} \quad (1)$$

where $\omega = 2\pi f$.

The governing equation of the pipe is then written as:

$$\bar{E} \frac{\partial^2 U_p(z,t)}{\partial z^2} + \frac{2\tau_{rz}(a,z,t)}{a} - \bar{\rho} \frac{\partial^2 U_p(z,t)}{\partial t^2} = -\frac{F_0}{A} \delta_p(z) e^{-i\omega t} \quad (2)$$

where $\tau_{rz}(a,z,t)$ represents the interactive shear stress at the interface.

With the assumptions stated above, together with the requirements on continuity of displacements at the pipe-medium interface, the boundary conditions on the medium displacements become

$$U_r(a,z,t) = 0, \quad U_z(a,z,t) = U_p(z,t) \quad (3a,b)$$

The dynamic displacements of the surrounding medium, $r \geq a$ may be expressed in terms of outgoing wave expressions (which decay as $r \rightarrow \infty$) as follows

[7]:

$$U_r(r,z,t) = \sum_{m=1}^{\infty} \left[A_m \frac{h_m^*}{h^2} H_1^{(1)}(h_m^* r) + B_m \frac{\alpha_m}{k^2} H_1^{(1)}(k_m^* r) \right] \sin \alpha_m z e^{-i\omega t} \quad (4)$$

$$U_z(r,z,t) = \sum_{m=1}^{\infty} \left[A_m \frac{\alpha_m}{h^2} H_0^{(1)}(h_m^* r) - B_m \frac{k_m^*}{k^2} H_0^{(1)}(k_m^* r) \right] \cos \alpha_m z e^{-i\omega t} \quad (5)$$

where $H_0^{(1)}$ and $H_1^{(1)}$ are Hankel functions of the first kind of order zero and one respectively,

$$\alpha_m = (2m-1)\pi/L, \quad (6)$$

$$h = \omega/c_p, \quad k = \omega/c_s, \quad (7a,b)$$

and

$$h_m^{*2} = h^2 - \alpha_m^2, \quad k_m^{*2} = k^2 - \alpha_m^2 \quad (8a,b)$$

In the above,

$$c_s = [\mu/\rho]^{1/2} \quad \text{and} \quad c_p = \left[\frac{2(1-\nu)}{1-2\nu} \cdot \frac{\mu}{\rho} \right]^{1/2} \quad (9a,b)$$

are the propagation speeds in an elastic medium of outgoing S- and P-waves respectively. Thus, the terms associated with the constants A_m represent the P-waves, while the B_m terms represent the propagation of the S-waves. The constants A_m and B_m must then satisfy the boundary conditions of Eq. (3).

From the first of these

$$B_m = - \left[\frac{h_m^*}{h^2} \frac{k^2}{\alpha_m} \frac{H_1^{(1)}(h_m^* a)}{H_1^{(1)}(k_m^* a)} \right] A_m \quad (10)$$

Furthermore, since $U_r(a, z) = 0$, the shear stress at the interface is given by

$$\tau_{rz}(a, z, t) = \mu \frac{\partial U_z(a, z, t)}{\partial r} \quad (11)$$

Using the remaining boundary condition, and substituting Eq. (11) in Eq. (2),

$$\bar{E} \frac{\partial^2 U_z(a, z, t)}{\partial z^2} + \frac{2\mu}{a} \frac{\partial U_z(a, z, t)}{\partial r} - \bar{\rho} \frac{\partial^2 U_z(a, z, t)}{\partial t^2} = - \frac{F_0}{A} \delta_p(z) e^{-i\omega t} \quad (12)$$

The periodic Dirac-delta function may now be represented in the region $0 \leq z \leq L$ by the infinite series

$$\delta_p(z) = \frac{2}{L} \sum_{m=1}^{\infty} \cos \alpha_m z \quad (13)$$

It is noted here in passing that the interval $0 \leq z \leq L$ represents a half-Fourier interval and hence the analysis of the infinite pipe is given by the solution in a periodic interval $0 \leq z \leq \lambda$ with $\lambda = 2L$ being the total Fourier interval [See Fig. (3)].

Noting that

$$\frac{dH_0^{(1)}(x)}{dx} = -H_1^{(1)}(x) \quad , \quad (14)$$

substituting the expression for U_z and its appropriate derivatives from Eq. (5) and using the representation of Eq. (13) in Eq. (12), we obtain, assuming a steady-state solution, the following equation:

$$\sum_{m=1}^{\infty} A_m \left\{ [\bar{E}\alpha_m^2 - \bar{\rho}\omega^2] D_{zm}(a) - \frac{2\mu}{a} g_m \right\} \cos \alpha_m z = \frac{2F_0}{AL} \sum_{m=1}^{\infty} \cos \alpha_m z \quad (15)$$

where

$$D_{zm}(r) = \frac{\alpha_m}{h^2} H_0^{(1)}(h_m^* r) + \frac{h_m^* k_m^*}{h^2 \alpha_m} \frac{H_1^{(1)}(h_m^* a)}{H_1^{(1)}(k_m^* a)} H_0^{(1)}(k_m^* r) \quad (16a)$$

and

$$g_m = \frac{\partial D_{zm}(r)}{\partial r} \Big|_{r=a} = - \frac{h_m^*}{h_m^2 \alpha_m} (\alpha_m^2 + k_m^{*2}) H_1^{(1)}(h_m^* a) \quad (16b)$$

By satisfying Eq. (15) term by term, the constants A_m are found, after some algebraic manipulation, to be

$$A_m = \frac{1}{G_m} \frac{2F_0 h^2}{\bar{E} A \alpha_m^3 L H_1^{(1)}(h_m^* a)} \quad (17a)$$

where

$$G_m = \left(1 - \frac{\omega^2}{c_m^2 \alpha_m^2}\right) \Lambda_m + \frac{2\mu}{\bar{E} a} \frac{h_m^*}{\alpha_m^4} (\alpha_m^2 + k_m^{*2}) \quad (17b)$$

and

$$\Lambda_m = \frac{H_0^{(1)}(h_m^* a)}{H_1^{(1)}(h_m^* a)} + \frac{h_m^* k_m^*}{\alpha_m^2} \frac{H_0^{(1)}(k_m^* a)}{H_1^{(1)}(k_m^* a)} \quad (17c)$$

In Eq. (17),

$$\bar{c} = [\bar{E}/\bar{\rho}]^{1/2} \quad (18)$$

represents the familiar propagation velocity of longitudinal waves in a free elastic rod.

Substituting finally Eqs. (17) in Eq. (5) and using Eq. (3b), the displacement $U_p(z,t)$ is obtained; viz

$$\left(\frac{U}{L}\right) \left(\frac{\bar{E} A}{F_0/2}\right) = \frac{4}{\pi^2} \sum_{m=1}^{\infty} \frac{\Lambda_m \cos \alpha_m z e^{-i\omega t}}{(2m-1)^2 G_m} \quad (19)$$

At this point it is advantageous to express the solution in terms of non-dimensional quantities and more specifically in terms of non-dimensional ratios relating the propagation velocities of the P- and S-waves in the medium and the propagation velocity \bar{c} of waves in the free bar. To this end, we define the following new non-dimensional variables:

$$\eta = a/\lambda \text{ where } \lambda = 2L \quad (20)$$

$$\Gamma = f\lambda/\bar{c} \quad , \quad (21)$$

and

$$R_c = c_p/c_s \quad , \quad R_v = c_p/\bar{c} \quad (22a,b)$$

Also, let the ratio of the densities of medium to pipe be

$$R_D = \rho/\bar{\rho} \quad (23)$$

Using these new parameters, the expression for the longitudinal displacement U_p of the bar becomes

$$\left(\frac{U}{L}\right) \left(\frac{\bar{E}A}{F_0/2}\right) = \frac{4}{\pi^2} \sum_{m=1}^{\infty} \frac{\cos \alpha_m z e^{-i\omega t}}{(2m-1)^2 - \Gamma^2 \left[1 - \frac{2R_D \gamma_{pm}}{(2\pi\eta)^2 (2m-1)^2 \Lambda_m} \right]} \quad (24)$$

where now

$$\Lambda_m = \frac{H_0^{(1)}(\gamma_{pm})}{H_1^{(1)}(\gamma_{pm})} + \frac{\gamma_{pm} \gamma_{sm}}{(2\pi\eta)^2 (2m-1)^2} \frac{H_0^{(1)}(\gamma_{sm})}{H_1^{(1)}(\gamma_{sm})} \quad (25)$$

in which

$$\gamma_{pm} = 2\pi\eta(2m-1) \left[\frac{\Gamma^2}{(2m-1)^2 R_v^2} - 1 \right]^{1/2} \quad (26)$$

and

$$\gamma_{sm} = 2\pi\eta(2m-1) \left[\frac{R_c^2 \Gamma^2}{(2m-1)^2 R_v^2} - 1 \right]^{1/2} \quad (27)$$

It is noted that the non-dimensional displacement given by Eq. (24) is uniquely determined by five quantities: Γ , R_D , R_v , and R_c , and η .

In the above, terms containing p and s subscripts correspond to contributions from the P- and S-waves respectively. Thus, it is observed that coupling of the two wave types occurs through Λ_m given in Eq. (25).

Certain limiting cases of the solution represented by Eq. (24) are of particular interest.

For example, noting that

$$\lim_{R_v \rightarrow 0} \frac{\gamma_{pm}}{\Lambda_m} = 0 \quad , \quad (28)$$

the solution degenerates to

$$\left(\frac{U}{L} \right) \left(\frac{\bar{E}A}{F_0/2} \right) = \frac{4}{\pi^2} \sum_{m=1}^{\infty} \frac{\cos \alpha_m z e^{-i\omega t}}{(2m-1)^2 - \Gamma^2} \quad (29)$$

Similarly if $R_D = 0$ or if $R_c \rightarrow \infty$ while both R_D and R_v remain finite, Eq. (29) is recovered from Eq. (24). The solution given by Eq. (29) is recognized as the solution for a free infinite bar with no interaction, i.e. as the uncoupled solution. In all three cases such a solution is expected since (a) $R_D = 0$ implies a massless soil, (b) $R_v = 0$ implies a soil of no rigidity and (c) $R_c \rightarrow \infty$ (with R_v , R_D finite) also implies a soil of no shear rigidity since,

$$\frac{R_v^2 R_D}{R_c^2} = \mu / \bar{E} \quad (30)$$

It is noted that for the response of the free bar, resonance occurs when

$$\Gamma = 2m-1 \quad , \quad m = 1, 2, 3\dots \quad (31a)$$

i.e. when the forcing frequency f is given by

$$f = \bar{c}/\lambda, 3\bar{c}/\lambda, 5\bar{c}/\lambda, 7\bar{c}/\lambda\dots \quad (31b)$$

It is thus convenient to define

$$\bar{f} = \bar{c}/\lambda \quad (32)$$

which is the fundamental frequency of vibrations of the uncoupled bar, or in terms of wave propagation, the wave frequency for a longitudinal wave of wave length λ propagating in the z -direction.

The variable Γ can then be rewritten as

$$\Gamma = f/\bar{f} \quad (33)$$

and thus represents the ratio of forcing frequency to natural frequency of the uncoupled free bar. This interpretation will subsequently prove significant in understanding the results presented in the next section.

The static solution for the interaction problem may also be recovered by letting f , or Γ , tend to zero. Noting that

$$\lim_{\Gamma \rightarrow 0} \gamma_{pm} = 2\pi\eta(2m-1)i(1-\epsilon/2) \quad (34a)$$

$$\lim_{\Gamma \rightarrow 0} \gamma_{sm} = 2\pi\eta(2m-1)i(1-R_c\epsilon/2) \quad (34b)$$

where

$$\epsilon = \left[\frac{\Gamma}{R_v(2m-1)} \right]^2 \ll 1 \quad (35)$$

and using the property [8]

$$H_n^{(1)}(ix) = \frac{2}{\pi} i^{-(n+1)} K_n(x), \quad (36)$$

upon taking the proper limits as $\Gamma \rightarrow 0$, the following expression is obtained

$$\left(\frac{U}{L}\right) \left(\frac{A\bar{E}}{F_0/2}\right) = \frac{4}{\pi^2} \sum_{m=1}^{\infty} \frac{\cos \alpha_m z}{(2m-1)^2 \left[1 + \frac{2R_D R_V^2}{v} \left\{ \frac{K_1^2(v)}{(R_c^2-1)[K_0^2(v)-K_1^2(v)] + 2R_c^2 K_0(v)K_1(v)} \right\} \right]} \quad (37)$$

where

$$v = 2\pi(2m-1)\eta \quad (38)$$

The functions $K_n(v)$ above are the modified Bessel function of order n .

This static solution, expressed in terms of the non-dimensional parameters, R_D , R_V , R_c is seen to be identical to that obtained directly using Love strain functions and given by eq. (18) of [9].

III. NUMERICAL RESULTS AND CONCLUSIONS - RADIATION DAMPING

Numerical results and conclusions are presented below for the displacements of a pipe, embedded in a typical soil, for a range of the various governing parameters.

All results were calculated for a soil having a Poisson ratio $\nu = 0.30$ and in which the propagation speed of shear waves $c_s = 400$ ft/sec. The ratio of the mass densities of soil to pipe was taken as $R_D = 0.20$ for all cases. The remaining parameters were chosen to simulate the

realistic condition of an infinite pipe of diameter D with flexible joints at regular intervals L . Thus, in considering the overall longitudinal stiffness of the jointed pipe, the global average modulus \bar{E} is so assumed that the wave frequency of longitudinal waves in a free pipe, $\bar{f} = \bar{c}/\lambda$, falls in the range from 1 Hz to 10 Hz, for the typical series of results with joints at periodic intervals $L = 20$ ft ($\lambda = 40$ ft).

From a study of seismographic readings, spectral analyses show that the significant components of major earth tremors fall within the range of frequencies $0.1 \text{ Hz} < f < 20 \text{ Hz}$. In order to study the dynamic effect of earthquakes on the pipe-soil system, the response to forces with given frequencies f is determined for a group of pipes having aspect ratios D/L in the realistic range $0.1 \leq D/L \leq 1.0$.

Significant results which demonstrate the dynamic effects on the displacements are best presented in terms of the ratio of the dynamic response U_D to the equivalent static response U_S , as obtained in [9].

The responses are therefore given in terms of the dynamic amplification factor

$$DAF = \frac{U_D(z=0)}{U_S(z=0)} \quad (39)$$

where the displacements $U_D(z=0)$ are evaluated from Eq. (24). Calculations of this quantity, using $M=15$ terms were found to insure sufficient accuracy in all cases.

In summary, the set of results presented are calculated with the following parameters held constant:

$$c_s = 400 \text{ ft/sec.}, \quad \nu = 0.3, \quad R_D = 0.2$$

and for aspect ratios $D/L = 0.1, 0.2, 0.4, 1.0$ (which correspond to values $\eta = 0.025, 0.05, 0.1, \text{ and } 0.25$ respectively). Three sub-series of results are presented, each sub-series representing a pipe with $\bar{f} = \bar{c}/\lambda$ as follows: (*)

$$(1) \quad \bar{f} = 1 \text{ Hz for which } R_v = 18.71$$

$$(2) \quad \bar{f} = 2 \text{ Hz for which } R_v = 9.357$$

$$(3) \quad \bar{f} = 10 \text{ Hz for which } R_v = 1.871$$

The response in each case is presented as a function of $\Gamma = f/\bar{f}$, with the other above parameters held fixed. Analogously to the definition of \bar{f} [as given in Eq. (32)], it is appropriate to define the equivalent wave frequency of the S- and P-waves propagating in the medium by

$$f_s = c_s/\lambda, \quad f_p = c_p/\lambda \quad (40a,b)$$

respectively. These frequencies are indicated in all figures presented below. It should be noted that from their definitions, $f_p = \bar{f}R_v$,

In Fig. (4) to Fig. (7), the DAF for the axial displacements are presented for $\bar{f} = 1$ Hz and for the various aspect ratios $D/L = 0.1, 0.2, 0.4, 1.0$ respectively. From these figures, it is seen that, aside from abrupt changes in behavior reflected, for example, by cusps at $f = f_p$, the behavior for small aspect ratios, say $D/L \leq 0.2$, is relatively smooth and the DAF are of the order of magnitude of unity. However, for larger aspect ratios D/L , the DAF occurring in the range $\bar{f} < f < f_p$ show sharp

(*) Note that $R_v \equiv c_p/\bar{c} = \left(\frac{2(1-\nu)}{1-2\nu}\right)^{1/2} \left(\frac{c_s}{\lambda}\right) \frac{1}{\bar{f}}$

peaks indicating an infinite response. (*) In the range $f_p < f$, however, the system will experience damping.

Before examining the next series of results, it is worthwhile to examine the damping mechanism and establish ranges of frequencies where such a damping mechanism exists. An understanding of the basic damping mechanism and resonant response is best obtained by examining Eqs. (4) and (5) which define the displacements of points in the surrounding soil. From these equations, it is observed that the displacement expressions contain terms of the nature $H_n^{(1)}(h_m^* r) e^{-i\omega t}$ and $H_n^{(1)}(k_m^* r) e^{-i\omega t}$, $n = 0$ and 1 , where h_m^* and k_m^* are originally defined by Eqs. (8). In terms of the new parameters given by Eqs. (20)-(22), (32) and (40), h_m^* and k_m^* are expressed respectively by

$$h_m^* = \frac{2\pi}{\lambda} \left[\frac{\Gamma^2}{(f_p/\bar{f})} 2^{-(2m-1)} \right]^{1/2} \quad (41a)$$

and

$$k_m^* = \frac{2\pi}{\lambda} \left[\frac{\Gamma^2}{(f_s/\bar{f})} 2^{-(2m-1)} \right]^{1/2} \quad (41b)$$

Thus, if $\Gamma > (2m-1)f_p/\bar{f}$, h_m^* is real, while if $\Gamma < (2m-1)f_p/\bar{f}$, h_m^* is imaginary. (Similar conclusions exist for k_m^* upon replacing f_p by f_s .)

(*) Resonance occurs, or there exist large DAF, when the frequency ratio Γ causes a denominator appearing in Eq. (24) to vanish or approach zero. The vanishing of such a denominator establishes the dispersion relation. From the dispersion relation it is thus possible to immediately determine frequencies at which resonance will take place.

In the case where h_m^* and k_m^* are real, the response is expressed in terms of Hankel functions of real arguments. Such terms then represent outward propagating waves in which energy is continuously propagated outwardly by the respective P- and S-waves. Thus, there exists, due to the outward radiation, a damping mechanism, and the system experiences radiation damping.

On the other hand, if the arguments of the Hankel functions are imaginary, the Hankel functions, in effect, are transformed into K_n functions, as seen in Eq. (36). The response, expressed then in terms of K_n functions, no longer is represented by radiating waves. Hence, no radiation of energy can take place and the system can experience no radiation damping.

Since the above discussion is applicable to both the h_m^* and k_m^* terms which correspond respectively to P- and S-waves, the following may be concluded:

- (a) If $(2m-1)f_p/\bar{f} < \Gamma$, radiation damping will take place through both the P- and S-wave mechanism.
- (b) If $(2m-1)f_s/\bar{f} < \Gamma < (2m-1)f_p/\bar{f}$, radiation damping will take place only through the S-wave mechanism.
- (c) If $\Gamma < (2m-1)f_s/\bar{f}$, no radiation damping can take place.

In Fig. (8) to Fig. (11), the response for identical parameters as in the first cases (R_D , ν , c_s , L , D/L) is presented with a frequency $\bar{f} = 2$ Hz. The behavior is observed to be similar to the case $\bar{f} = 1$ Hz.

In Fig. (12) to Fig. (15) the corresponding response for $\bar{f} = 10$ Hz is given. It is noted that as \bar{f} increases, with other parameters held constant, the response becomes smoother and fewer cases of undamped resonant behavior take place.

In conclusion, the results presented show several trends in the frequency ranges encountered in earthquakes, which may be summarized as follows:

- (a) The DAF for pipes having relatively low aspect ratios, (e.g. $D/L < 0.2$) will not contain sharp peaks in response to earthquakes where low frequencies predominate.
- (b) As D/L increases, the resonant response becomes more significant, and relatively large DAF are encountered.
- (c) High resonant responses will occur at low frequencies due to an absence of radiation damping. Such responses will tend to occur for pipe-soil systems where $f_s = c_s/\lambda$ is relatively large; i.e. in relatively stiff soils containing pipes with joints spaced relatively closely.

REFERENCES

1. "Proceedings of U.S.-Japan Seminar on Earthquake Engineering Research With Emphasis on Lifeline Systems," Tokyo, 1976.
2. "The Current State of Knowledge of Lifeline Earthquake Engineering," Proceedings, Technical Council on Lifeline Earthquake Engineering Specialty Conference, University of California at Los Angeles, ASCE, 1977.
3. "Lifeline Earthquake Engineering - Buried Pipelines, Seismic Risk, and Instrumentation," Third National Congress on Pressure Vessels and Piping, San Francisco, ASME, 1979.
4. Shinozuka, M. and Koike, T., "Estimation of Structural Strains in Underground Lifeline Pipes," Columbia University Technical Report No. NSF-PFR-78-15049-CU-4, NSF Grant No. NSF-PFR-78-15049, March 1979. (See also [3], pp. 31-48.)
5. O'Rourke, M.J. and Wang, L. R-L, "Earthquake Response of Buried Pipelines," R.P.I. Technical Report No. 4, NSF Grant No. ENV 76-14884, March 1978.
6. Weidlinger, P. and Nelson, I., "Seismic Analysis of Pipelines with Interference Response Spectra," NSF Grant Report GR-7, Weidlinger Associates, June 1978.
7. Toki, K. and Takada, S., "Earthquake Response Analysis of Underground Tubular Structures," Bull. Disas. Prev. Res. Inst., Kyoto University, Vol. 24, No. 221, June 1964.
8. McLachlan, N.W., "Bessel Functions for Engineers," Oxford, 1955.
9. Parnes, R., "Static Analysis of an Embedded Pipe Subjected to Periodically Spaced Longitudinal Forces," NSF Grant Report GR-12, Weidlinger Associates, August 1979.



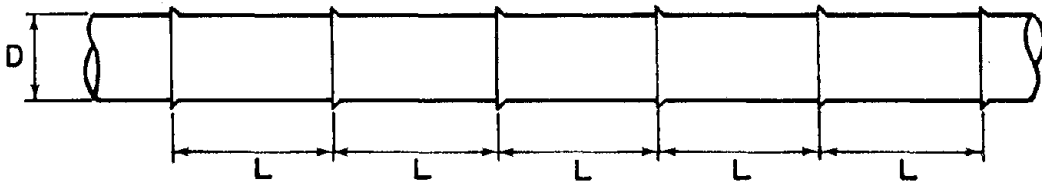


Fig (1)

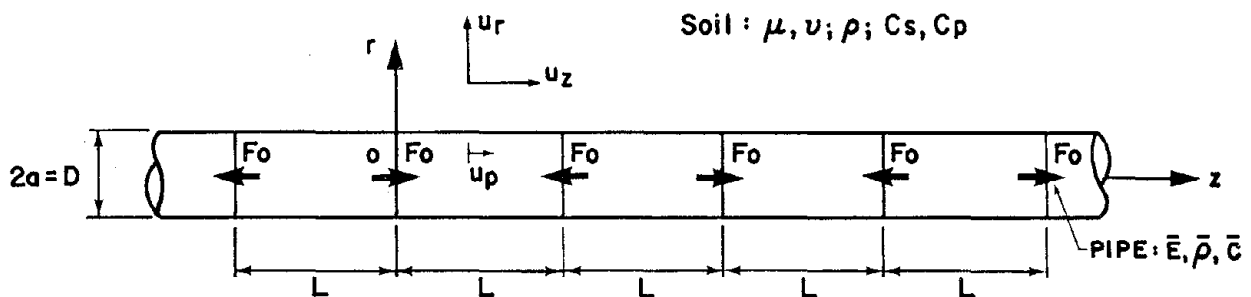


Fig (2)

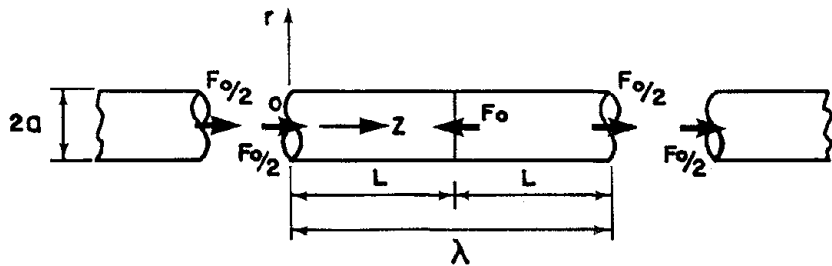
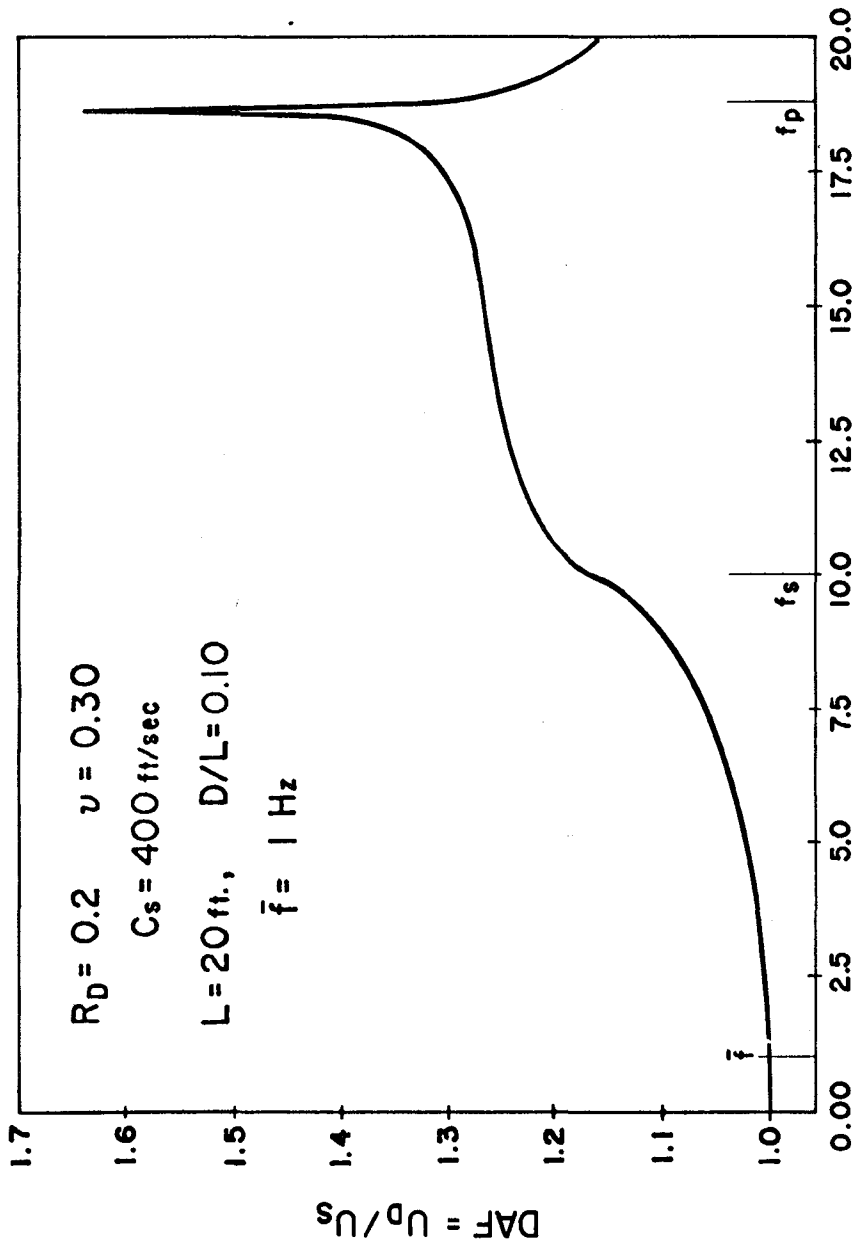
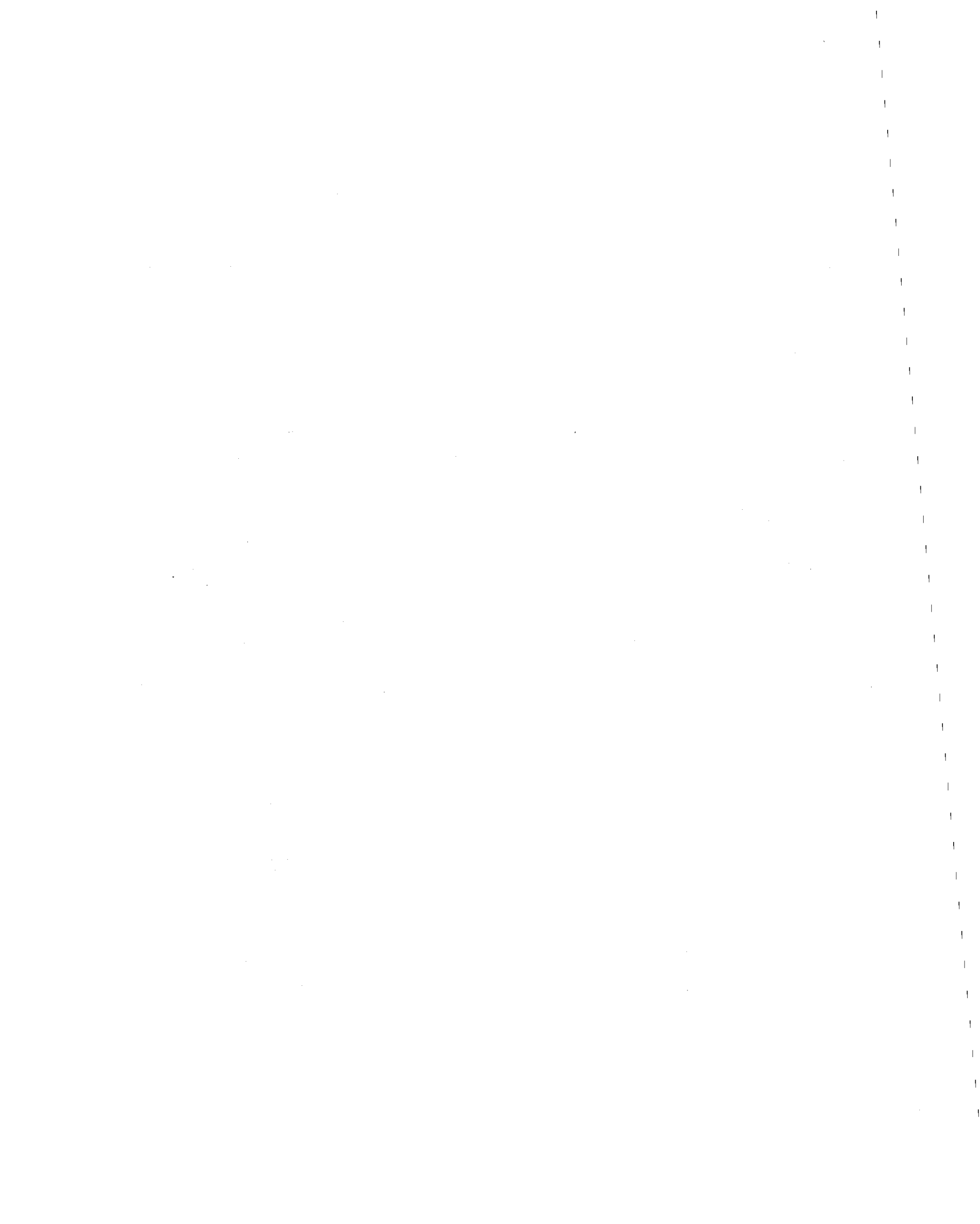


Fig (3)





$\Gamma = f / \bar{f}$
 Fig. 4



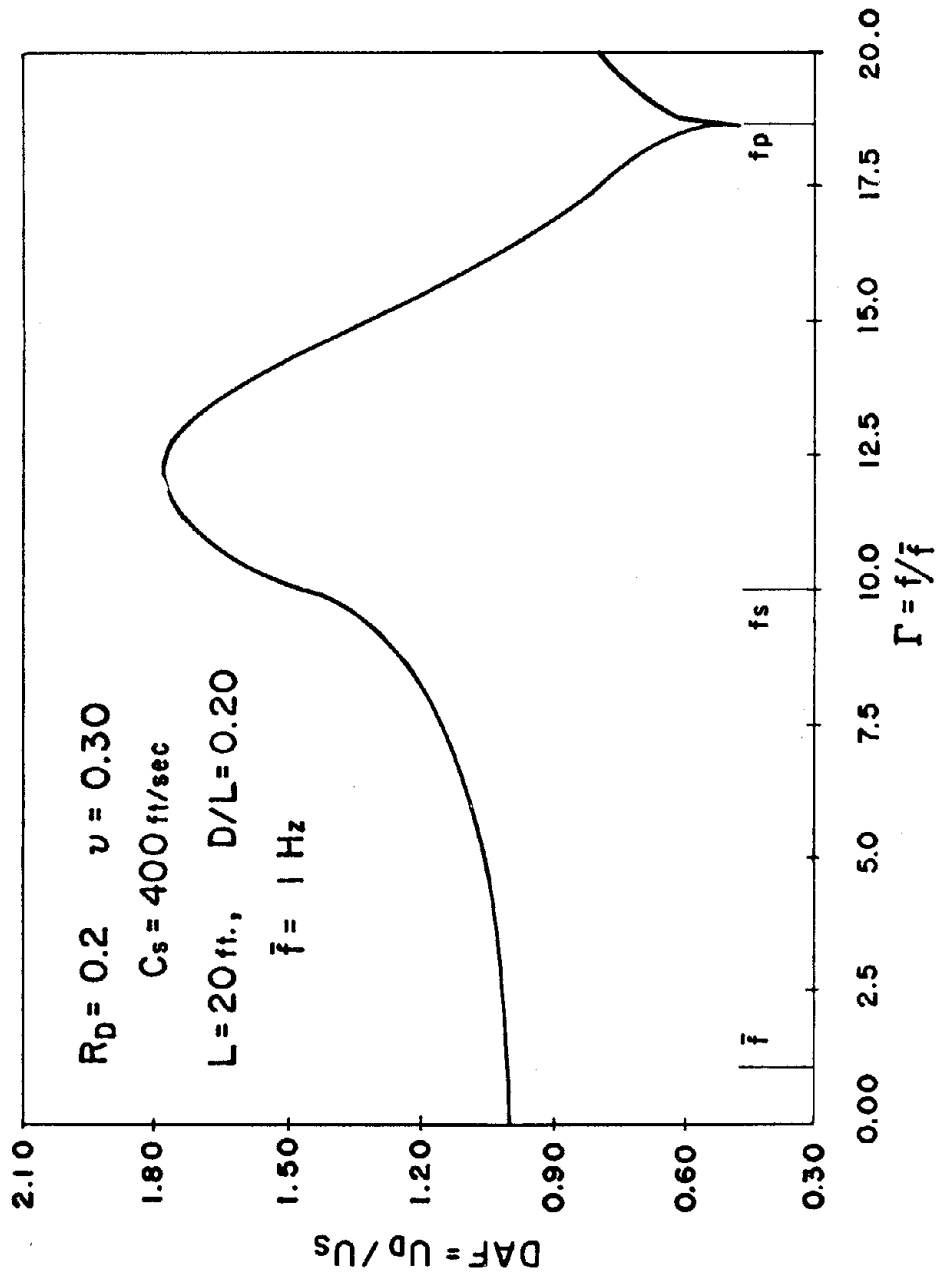
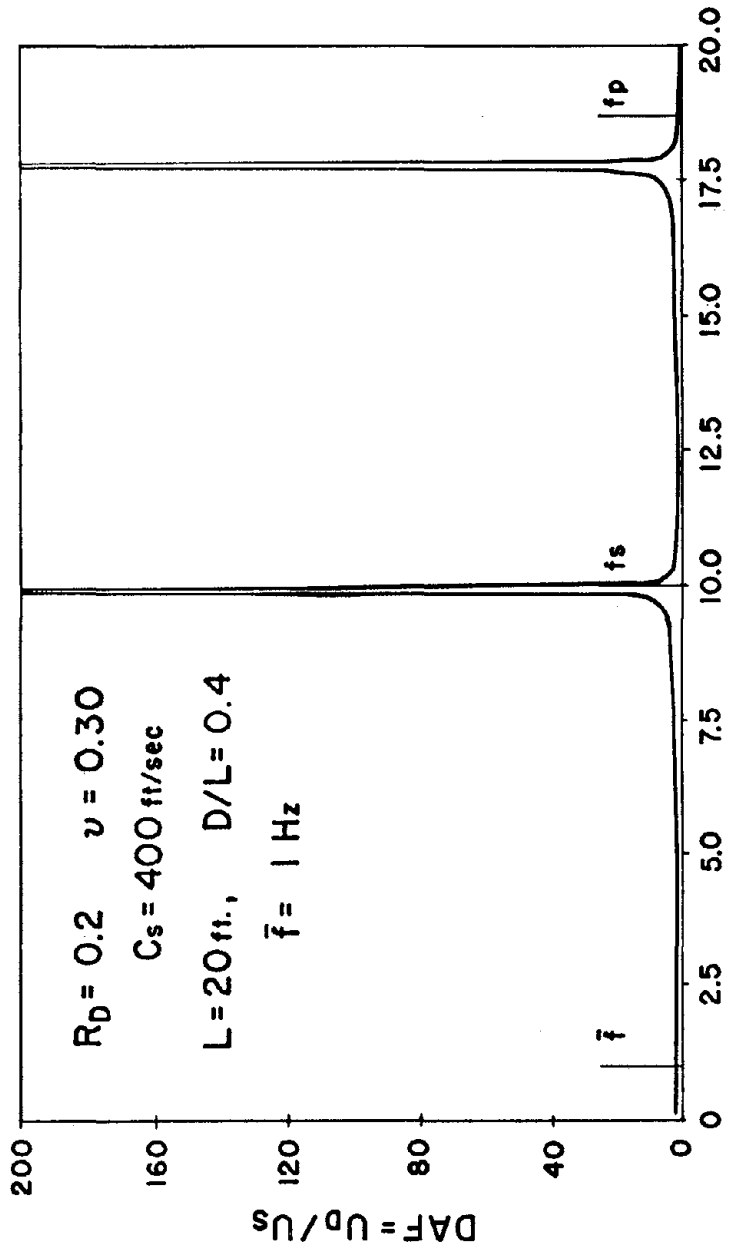


Fig. 5



$\Gamma = f / \bar{f}$

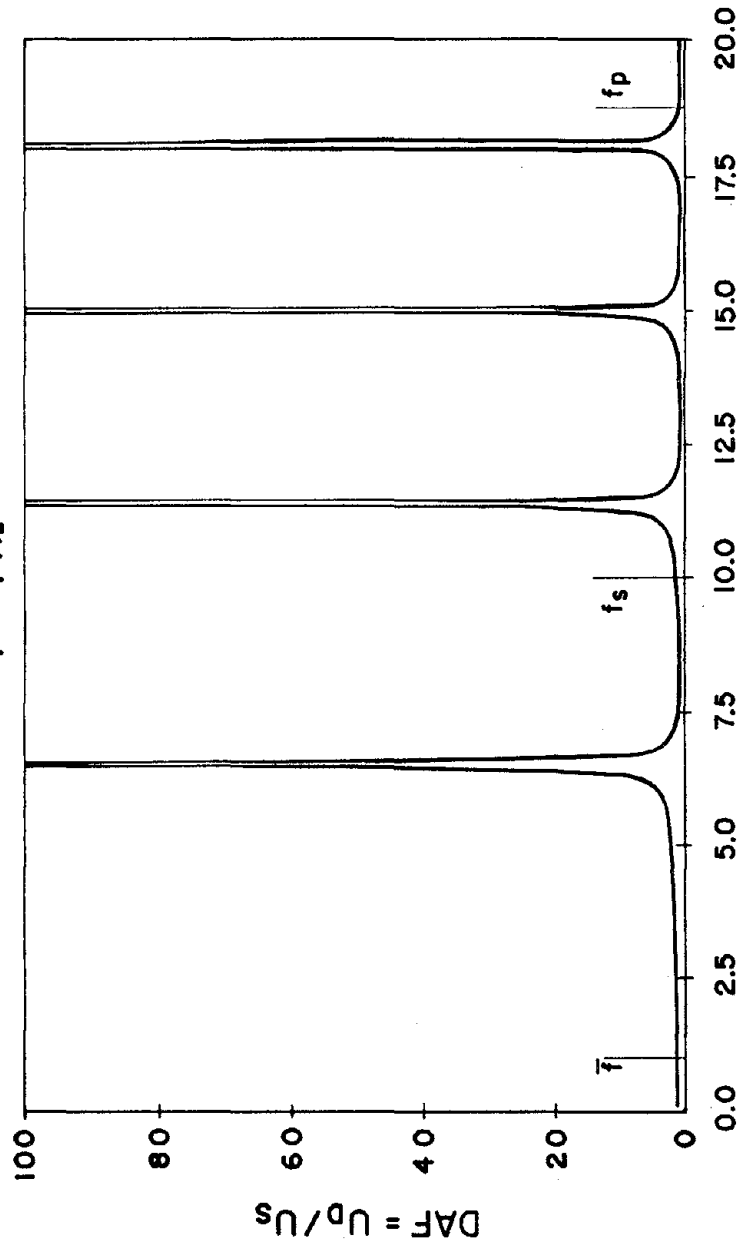
Fig. 6

$$R_D = 0.2 \quad \nu = 0.30$$

$$C_s = 400 \text{ ft/sec}$$

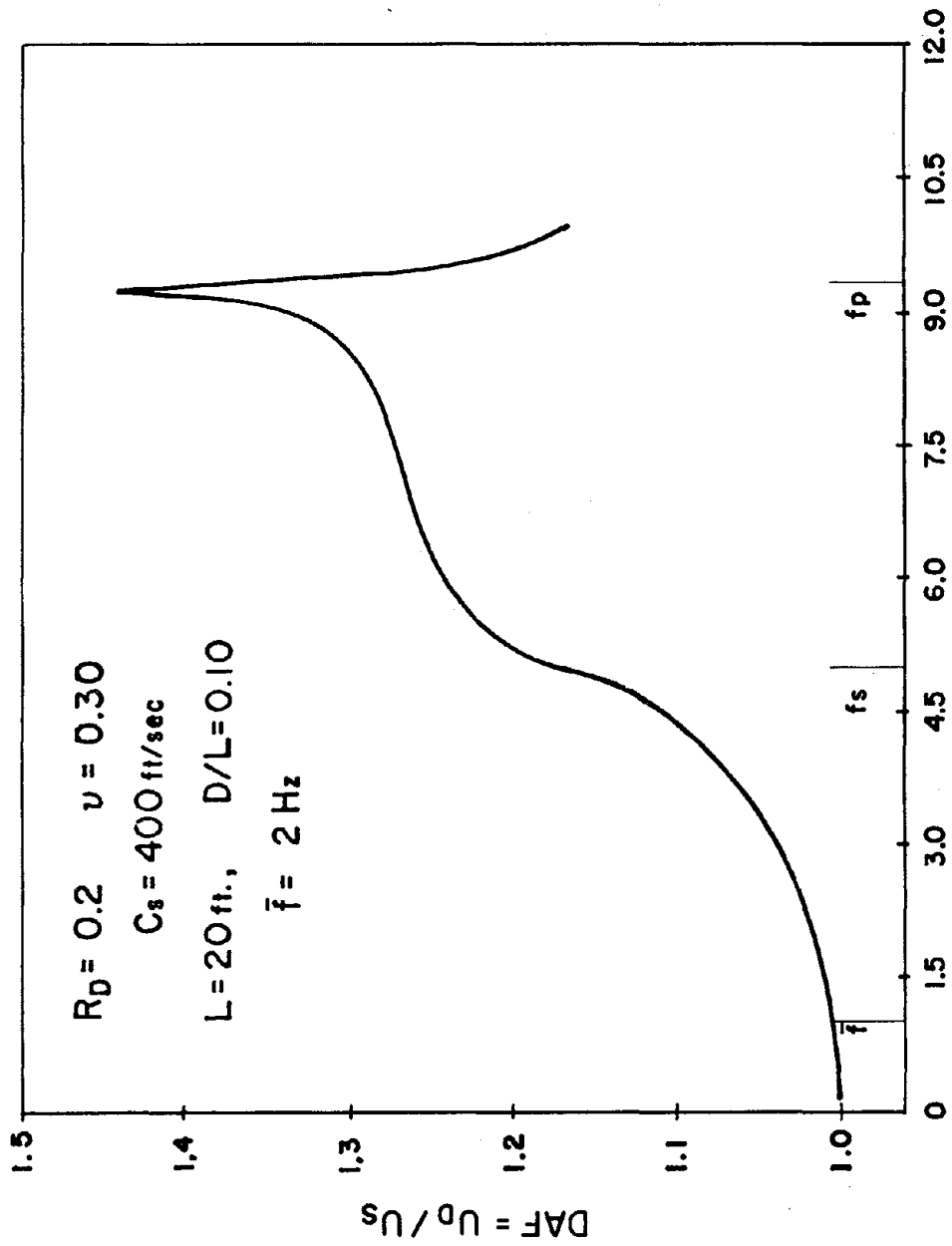
$$L = 20 \text{ ft.}, \quad D/L = 1.0$$

$$\bar{f} = 1 \text{ Hz}$$



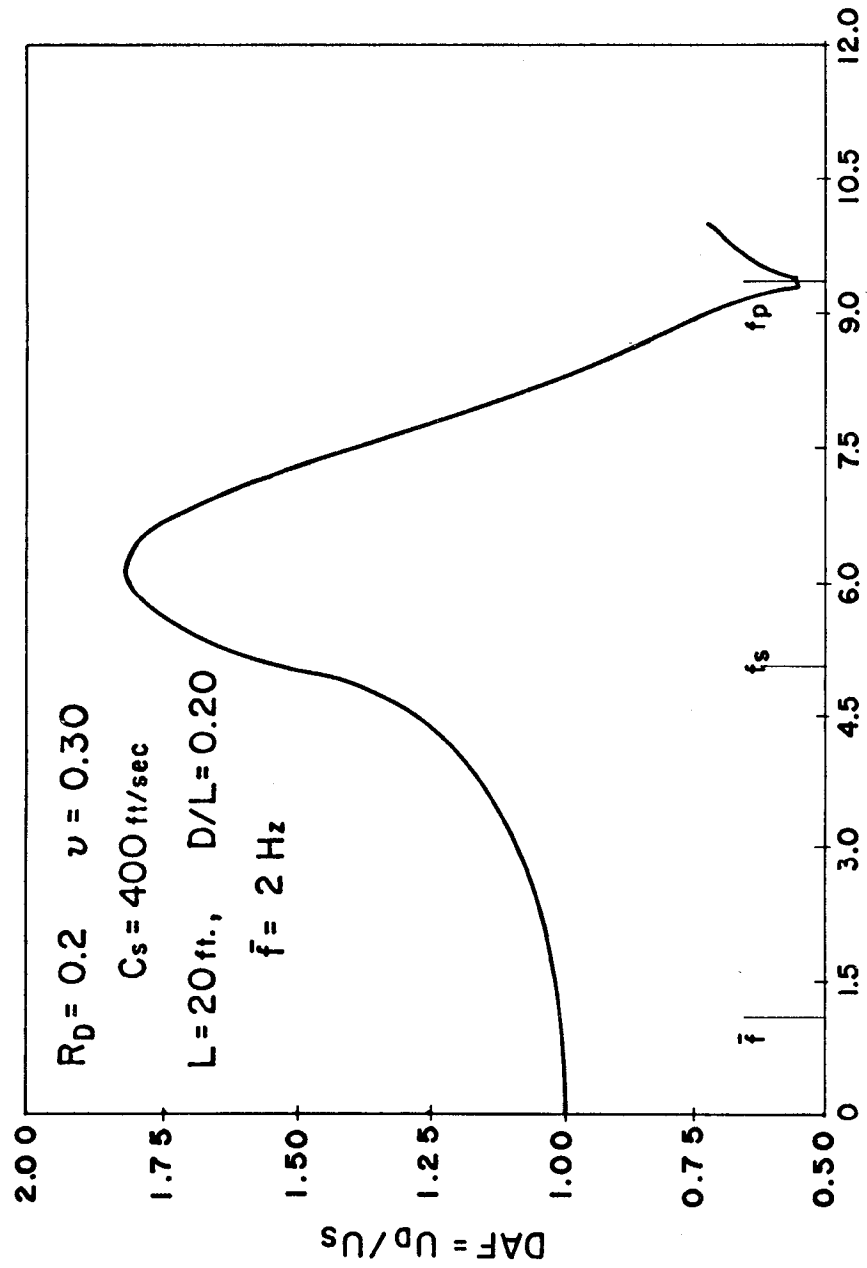
$$\Gamma = f/\bar{f}$$

Fig. 7



$T = f/\bar{f}$
 Fig. 8





$\Gamma = f/\bar{f}$
 Fig. 9

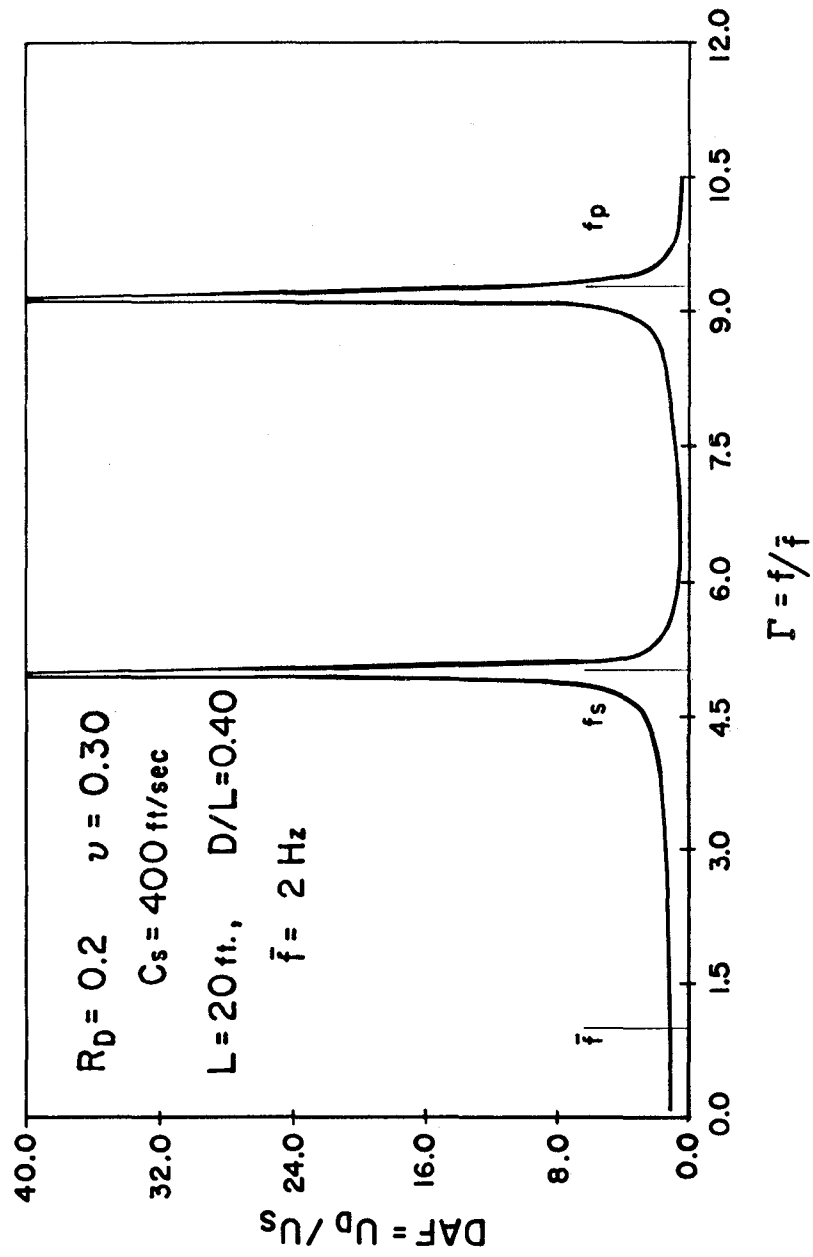
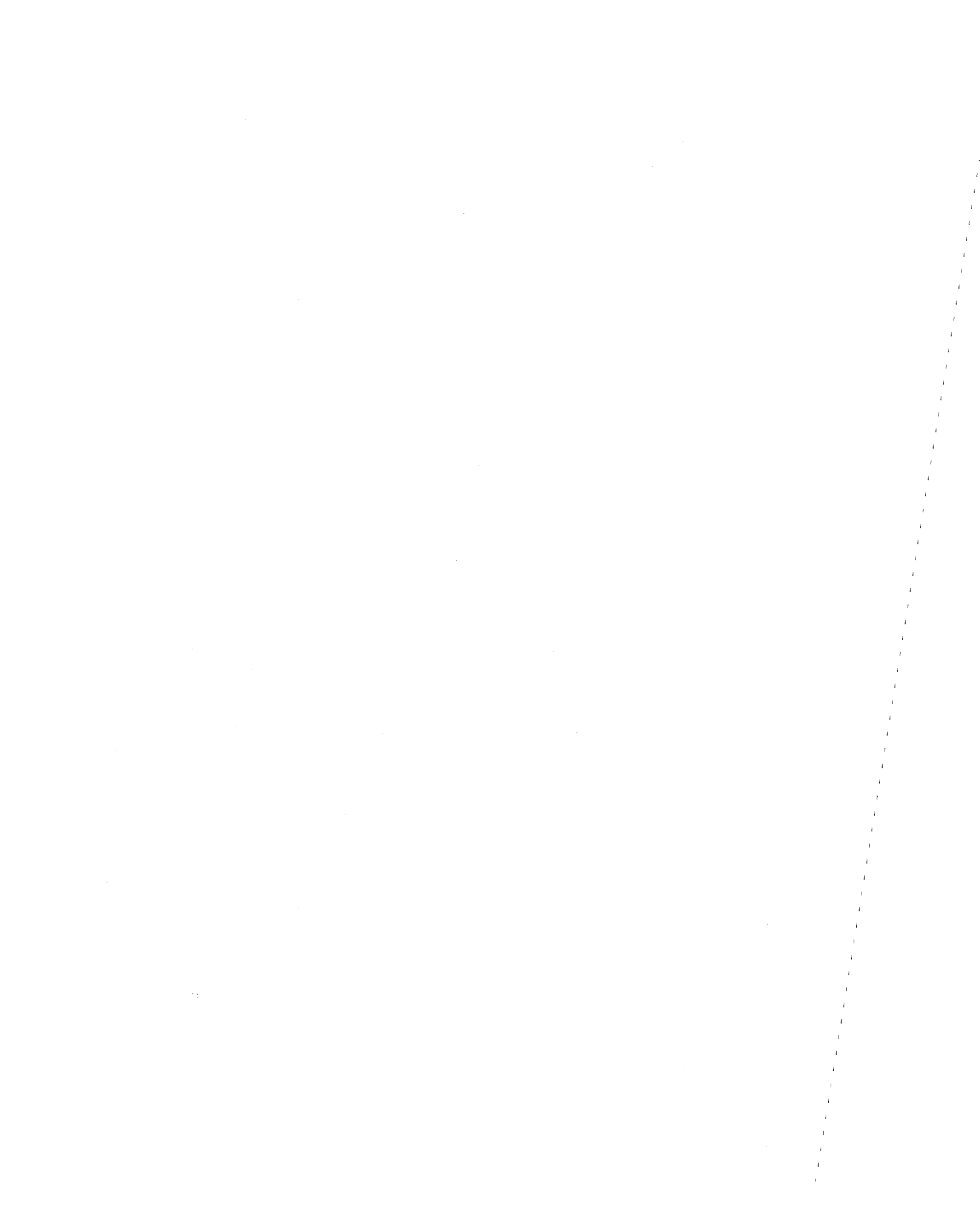


Fig. 10



$$R_D = 0.2 \quad \nu = 0.30$$

$$C_s = 400 \text{ ft/sec}$$

$$L = 20 \text{ ft.}, \quad D/L = 1.0$$

$$\bar{f} = 2 \text{ Hz}$$

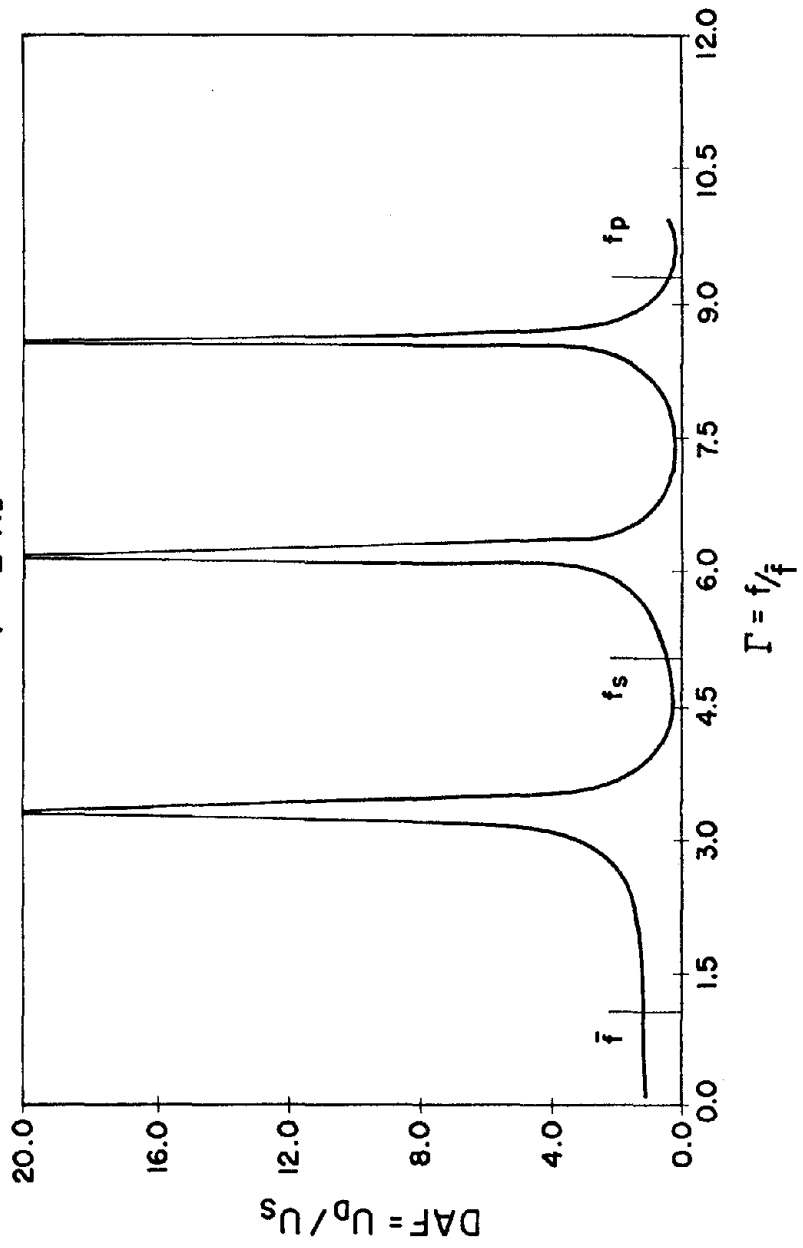


Fig. II

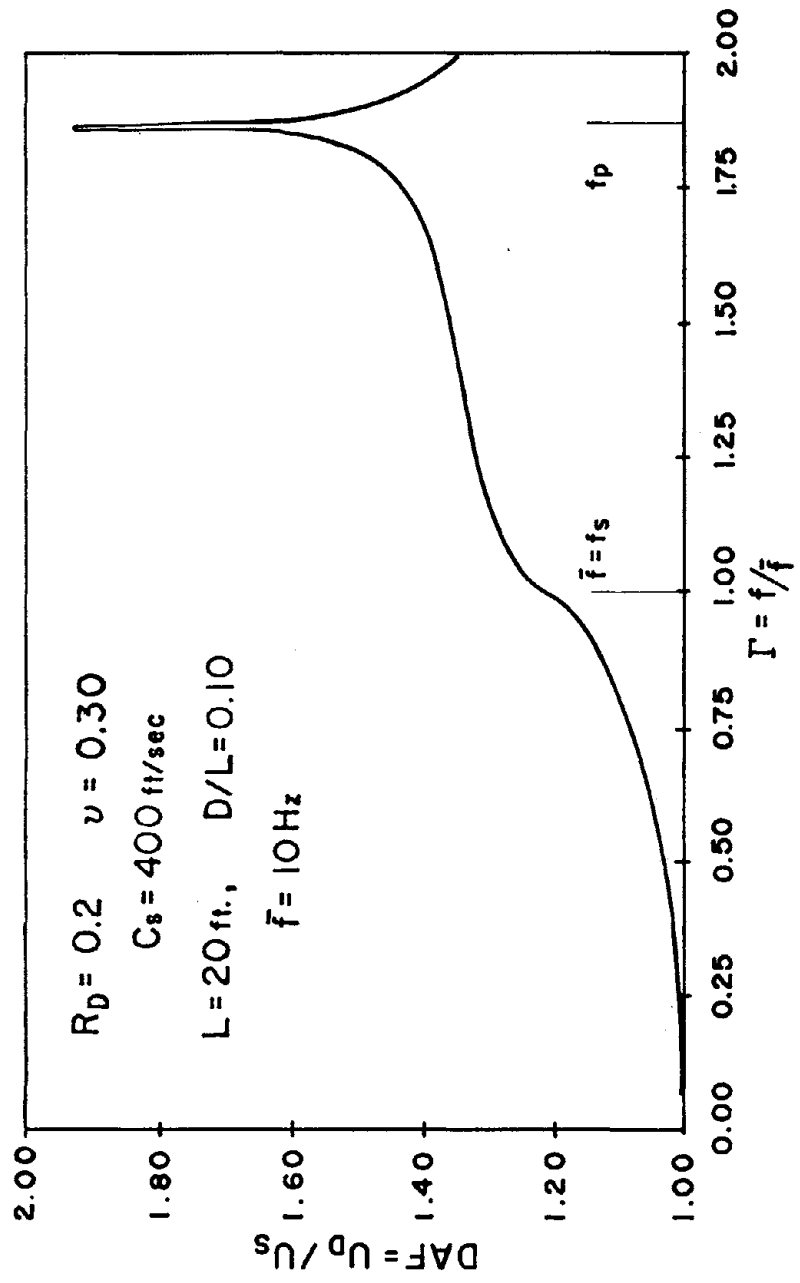
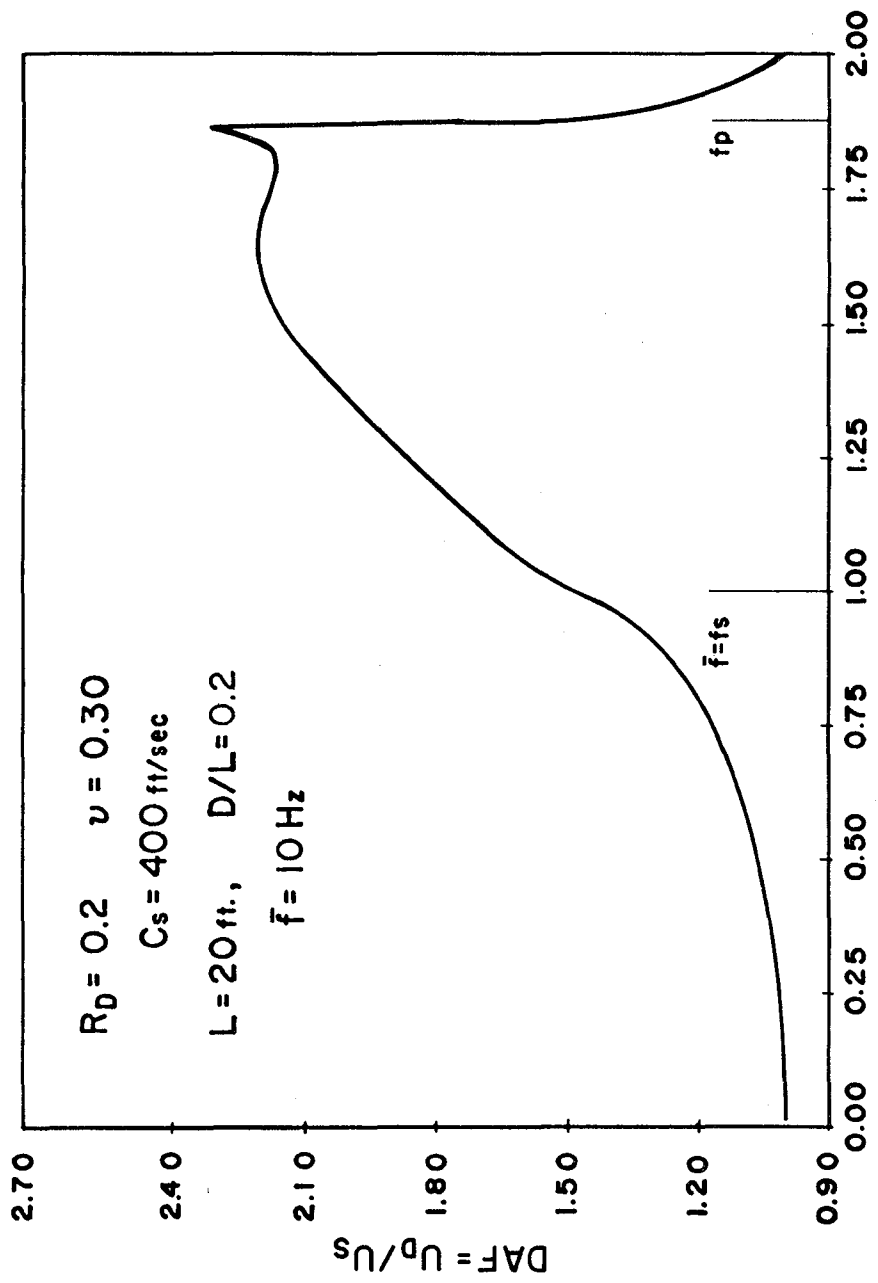
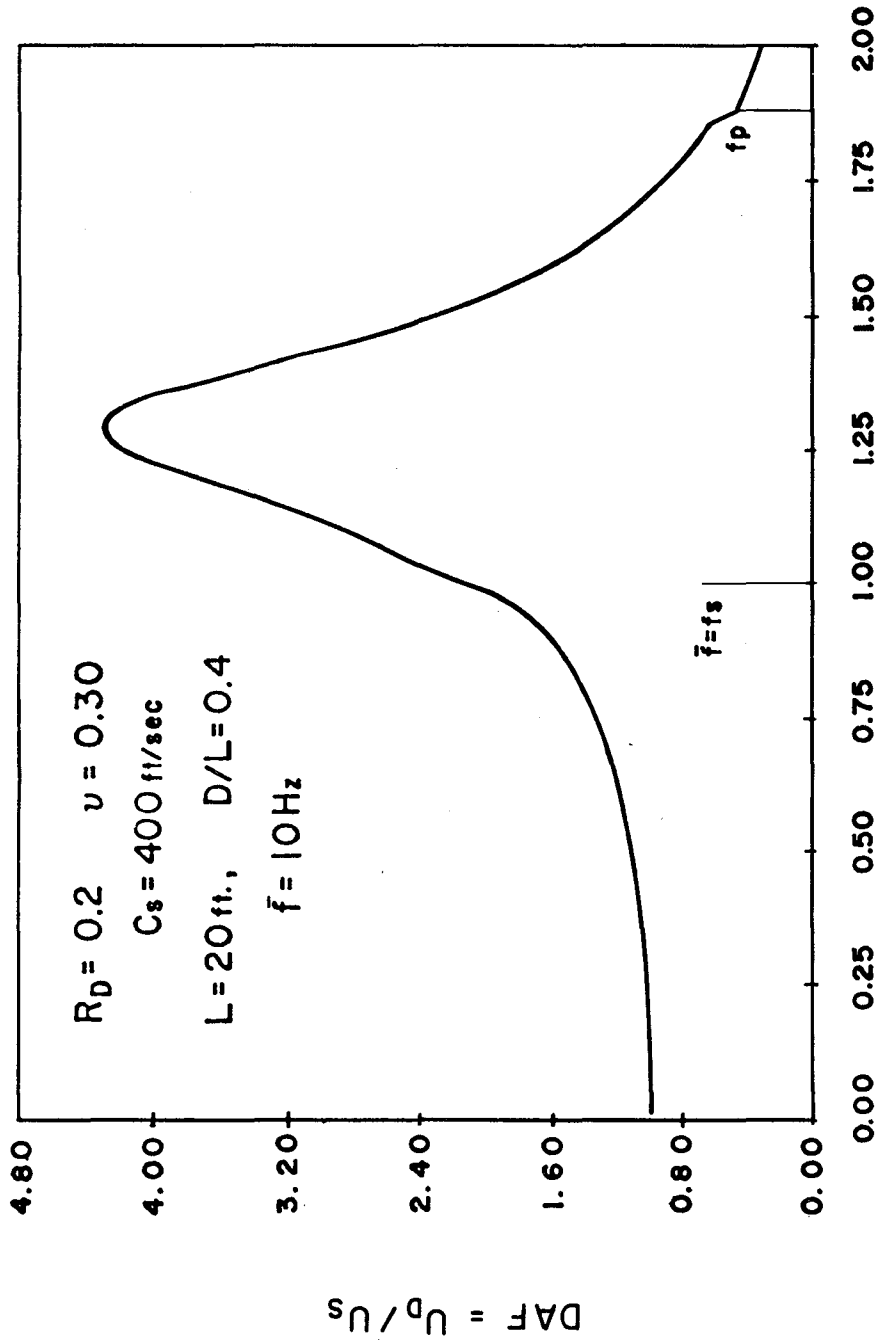


Fig. 12



$\Gamma = f/\bar{f}$

Fig. 13



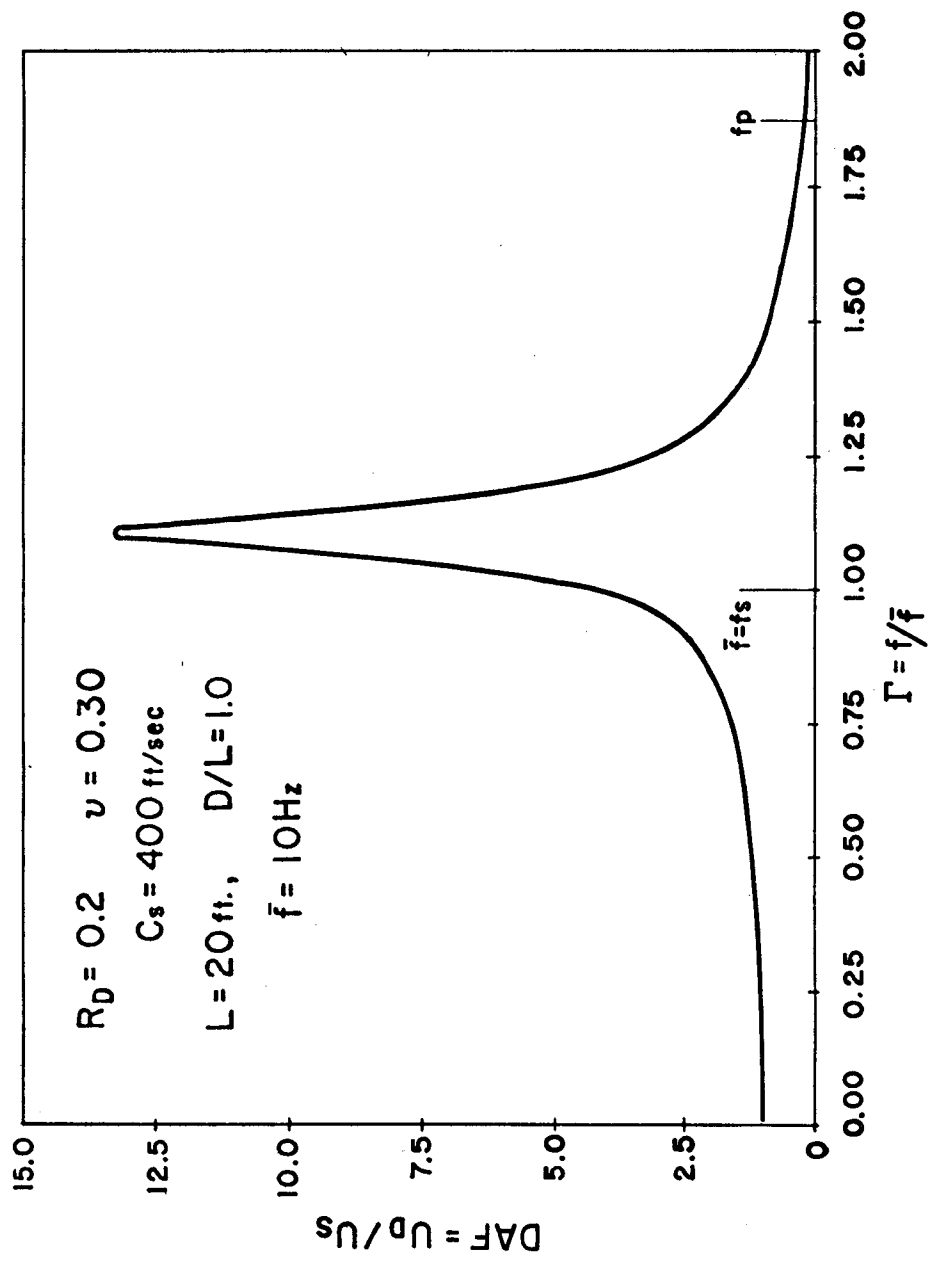


Fig. 15

